Astronomy & Astrophysics manuscript no. oka
(DOI: will be inserted by hand later)

Numerical Simulation of the Surface Flow on the Companion Star in a Close Binary System

II. Construction of Doppler maps and application to Galactic supersoft X-ray sources

Kazutaka Oka[1], Takuya Matsuda[1], Izumi Hachisu[2] and Henri M.J. Boffin[3]

[1] Department of Earth and Planetary Sciences, Kobe University, Kobe, 657-8501, Japan
e-mail: kazutaka@kobe-u.ac.jp, tmatsuda@kobe-u.ac.jp
[2] Department of Earth Science and Astronomy, College of Arts and Sciences, University of Tokyo, Komaba, Meguro-ku, Tokyo 153-8902, Japan
e-mail: hachisu@chianti.c.u-tokyo.ac.jp
[3] European Southern Observatory, Karl-Schwarzschild-Str. 2, D-85748 Garching-bei-München, Germany
e-mail: hboffin@eso.org

the date of receipt and acceptance should be inserted later

Abstract. We perform three-dimensional numerical simulations of surface flows on the companion star in a semi-detached binary system and construct the corresponding Doppler maps. The mass ratio of the binary system, $q = M_2/M_1$, considered here is $q = 0.05, 0.33, 0.5, 1, 2$, and 3. For all cases, we obtain the H-, L1-, and L2-eddies, as found in our previous work, and confirm that the flow pattern does not heavily depend on the mass ratio. We propose that this kind of problem be dubbed "*stellar meteorology*." The Doppler maps at the position of the companion show a structure tilted towards clockwise direction and presenting deviations from the critical Roche surface due to the L1-eddy and the L2-eddy on the companion star.
We apply our results to the Galactic supersoft X-ray source RX J0019.8+2156 and try to attribute the low radial velocity component of the emission lines of He II λ4686 observed recently to the irradiated spot on the surface of the companion rather than that of the white dwarf or the accretion disc. Based on the comparison between the observations and our constructed Doppler map, we estimate the mass of the companion star in RX J0019.8+2156 to be $\sim 2M_\odot$ assuming the mass of the white dwarf star to be around $0.6M_\odot$.

Key words. binaries: close – star: evolution – stars: mass-loss – stars: emission-line – stars: individual (RX J0019.8+2156) – stars: winds, outflows – X-rays: stars – accretion, accretion discs

1. Introduction

A semi-detached binary system consists of a Roche-lobe-filling companion star and a (compact) accreting object. Part of the gas of the companion star is gravitationally attracted by the primary, flows through the L1 point towards the primary star and, if the latter is smaller than the circularisation radius, forms an accretion disc around it.

Many studies on the accretion disc itself exist, but until recently, only a very few studies considered the surface flow of the companion, except for the pioneering work by Lubow & Shu (1975). A possible reason for the lack of studies on the companion is that there had been no effective way to observe the surface of the companion star as well as the flow on it.

However, Davey & Smith (1992) demonstrated the surface mapping method of the companion surface in cataclysmic variables (CVs) using Na I line absorption. Dhillon & Watson (2000) demonstrated a technique of imaging companion stars of CVs using Roche tomography. Besides, Doppler map technique also can potentially give some trace of the surface flow (as considered in this paper).

Oka et al. (2002) performed three-dimensional simulations of surface flows on the companion star and predicted the existence of three kinds of eddy associated with a high/low pressure on the companion star: the H-, L1-, and L2-eddies as schematically shown in Fig.1. The notations H, L1 and L2 denote the high pressure around a (north) pole, the low pressure around the L1 point and the low pressure at the opposite side to the L1 point, respectively.

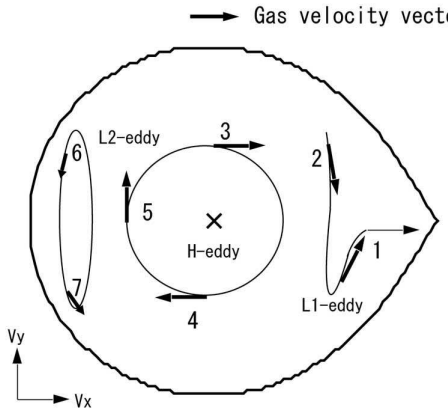

Fig. 1. A schematic diagram of the surface flow of a companion star in a semi-detached binary system: H, L1 and L2 denote eddies associated with a high/low pressure, respectively. Typical velocity vectors are shown with numbers.

In a rotating fluid, the pressure gradient force balances the Coriolis force, and the wind blows thus along isobaric lines. On the Earth, such a flow is called the geostrophic wind, while on a star it was called the astrostrophic wind by Lubow & Shu (1975). Therefore, a clockwise-rotating eddy forms around a high pressure region, while a counterclockwise rotating eddy appears around a low pressure region on the northern hemisphere in our counterclockwise rotating system (viewed from the north). We dub this kind of problem "*stellar meteorology*."

With the observational progress mentioned above as well as theoretical ones in hand, we are now in the state of investigating the flow on the surface of the companion star in some more detail.

Oka et al. (2002) considered only the mass ratio of unity. In reality, however, the range of mass ratio is wide, and it is thus interesting to investigate the dependence of the flow pattern on the mass ratio, $q = M_2/M_1$. In the present study, we consider six cases for the mass ratio: $q = 0.05, 0.33, 0.5, 1, 2$, and 3. As described above, a Doppler map can potentially give some traces of the surface flow, and so we construct Doppler maps in the present study as well.

1.1. Observational implication of the surface flow on the companion star

Davey & Smith (1992) found an asymmetric irradiation pattern in the secondary star of dwarf novae (e.g. IP Peg); the trailing hemisphere has stronger Na I line absorption than the leading hemisphere (see also Dhillon & Watson 2000). They considered that this asymmetry could be due to the circulation current on the companion star (but see Watson et al. 2003).

As was stated above, Oka et al. (2002) found three types of eddies on the companion star. They considered that the H-eddy as well as the L1-eddy could transport the heat due to the irradiation to the leading hemisphere, and argued that these currents naturally explained the asymmetry of the irradiation pattern. Note, however, that magnetic CVs, on the other hand, show the irradiation to be on the trailing hemisphere (Davey & Smith 1992,1996; Watson et al. 2003). To understand the irradiation pattern of magnetic CVs, we need another mechanism, which could lead to the effective heating of the trailing hemisphere.

1.2. Supersoft X-ray sources

Supersoft X-ray sources (SSS) consist, like CVs, of a Roche lobe filling companion star and a white dwarf. X-rays are believed to be produced by a steady nuclear burning occurring on the surface of the white dwarf. This requires a high mass accretion rate ($\gtrsim 10^{-7} M_\odot$/yr) that is only possible with a high mass companion star (van den Heuvel et al. 1992).

In our galaxy four SSSs are known (see e.g. Gänsicke et al. 2000); one of which is RX J0019.8+2156. This object and its 12.2 mag optical counterpart were discovered by Beuermann et al. (1995). Recent observations revealed a low radial velocity component to the He II λ4686 emission line (e.g. Becker et al. 1998; Cowley et al. 1998; Deufel et al. 1999; McGrath et al. 2001). These authors considered that the He II λ4686 emission line was emitted from the white dwarf or from the inner part of the accretion disc. With this assumption they estimated the mass of the companion to be smaller than the white dwarf. However, this estimate certainly contradicts the massive companion theory developed by van den Heuvel et al. (1992).

Hachisu & Kato (2003), on the other hand, considered that the low radial velocity of the He II λ4686 emission line was emitted from the inner hemisphere of the companion star. The inner hemisphere is irradiated by the companion and becomes hot enough to emit the He II λ4686 line. The Doppler map of He II λ4686 observed by Deufel et al. (1999) showed that the emission line peak is located around $V_{\rm x} \sim$ 100 km/s and $V_{\rm y} \sim$ 100 km/s (Note that the plus sign of the above velocity is due to our choice of the coordinate frame). This emission line peak does not correspond to the region of the white dwarf or the inner part of the accretion disc. With the irradiated companion model Hachisu & Kato (2003) argued that such low radial velocity emission lines were naturally explained by the massive companion star in a system with a mass ratio of $q \sim 3-4$ and a white dwarf of $0.6 M_\odot$.

Matsumoto & Mennickent (2000) constructed the Doppler map of He II λ4686 of RX J0925.5-4758 which is another known Galactic SSS and also found a peak located around $V_{\rm x} \sim$ 100 km/s and $V_{\rm y} \sim$ 100 km/s (in our velocity sign): i.e., the low radial velocity region. The low

Table 1. Mass ratio, computational region, and number of grid points of models

Mass ratio	Computed region	Number of grid points
0.05	$1.0 \times 1.0 \times 0.5$	$101 \times 101 \times 51$
0.33	$1.0 \times 1.0 \times 0.5$	$101 \times 101 \times 51$
0.5	$1.1 \times 1.0 \times 0.5$	$111 \times 101 \times 51$
1	$1.2 \times 1.0 \times 0.5$	$121 \times 101 \times 51$
2	$1.4 \times 1.2 \times 0.6$	$141 \times 121 \times 61$
3	$1.4 \times 1.2 \times 0.6$	$141 \times 121 \times 61$

velocity of the He II λ4686 emission line seems therefore to be a common feature of supersoft X-ray sources.

Hachisu & Kato (2003) tried to interpret the low radial velocity component of the He II λ4686 emission line in the Doppler map of RX J0019.8+2156. However, their numerical model was two-dimensional, and could therefore not handle flows on the surface of the companion. A three-dimensional calculation is necessary in this respect, and this is the aim of the present research.

This paper is organized as follows. In Sect. 2 we describe the assumptions of the model and the numerical method. In Sect. 3 we show the flow patterns and construct Doppler maps. In Sect. 4 we discuss the problem of the supersoft X-ray sources. A discussion and a summary are given in Sect. 5.

2. Assumptions and Numerical Method

2.1. Assumptions

The binary system considered here consists of a primary compact star with mass M_1 and a companion star with mass M_2. The system rotates counter-clockwise viewed from the north. The mass ratio of the binary system is defined by $q = M_2/M_1$.

We solve the three-dimensional Euler equations in the rotating frame of the binary. The equation of state considered here is that of an ideal gas characterized by a specific heat ratio γ. Complex effects such as physical/turbulent viscosity (except numerical one), magnetic fields, and irradiation from the accretion disc or the primary star are neglected.

The equations are normalized with length by the separation A between the centres of two stars, and time by $1/\Omega$, where Ω denotes the orbital angular velocity of the binary system and, therefore, the orbital period equals 2π. The density on the inner (numerical) boundary is taken to be unity. The gravitational constant G is eliminated using the above normalization.

2.2. Numerical method

We use a Cartesian coordinate system. The origin of the coordinate is located at the centre of the primary star. The x-axis coincides with the line joining the centres of the two stars. We define the $x-y$ plane as the orbital plane, so that the z-axis is perpendicular to the orbital plane and is oriented in the same direction as the angular momentum vector of the orbital rotation. Note that we put the mass-donor star in the negative x domain following our convention; other authors seem to prefer to put it in the positive x domain. Therefore, our sign of velocity is different from the convention of many other authors.

The computational region is a rectangular box, and its size and the number of grid points depend on the cases as described below. We assume symmetry about the orbital plane, and thus only the upper half of the region is computed. We use the simplified flux splitting (SFS) technique proposed by Jyounouchi et al. (1993) and Shima & Jyounouchi (1994) as a Riemann solver, and the MUSCL-type technique is used as an interpolation. The method is the same as in Makita et al. (2000), Matsuda et al. (2000), Fujiwara et al. (2001) and Oka et al. (2002). The spatial and temporal accuracy are kept at second-order levels.

2.3. Boundary and initial conditions

We apply the same boundary conditions as in Oka et al. (2002). The inner boundary is assumed to be an equipotential surface slightly smaller than the critical Roche lobe ($\sim 90\%$ of the critical Roche lobe radius) of the companion. Note that this inner boundary does not necessarily mean the real surface of the companion, but is chosen for numerical reasons.

The inside of the companion star is filled with a gas with zero velocity, density $\rho_0 = 1$, and sound speed c_0, where c_0 is a free parameter. We mainly examine the case of $c_0 = 0.05$. The gas can naturally flow out from the inner boundary if the gas pressure below the inner boundary is higher than above it.

The outside of the outer boundary is assumed to be always filled by a gas of fixed velocity, 0, density, ρ_1, and sound speed c_1, where ρ_1 and c_1 are parameters that are taken to be 10^{-5} and $\sqrt{10}$, respectively. We note that for the calculation of the accretion discs with q=1, 2, and 3, the density of the initial ambient gas ($\rho_1 = -5$) is somewhat large, and therefore affects the accretion discs. In order to reduce the effect of the initial ambient gas we use a much lower ambient gas density of $\rho_1 = -7$ when q is 1, 2, and 3.

At the initial time $t = 0$, the entire region, except the inside of the inner boundary, is occupied by a gas with velocity 0, ρ_1, and c_1. We follow the time evolution until a steady state is reached. We describe only steady states in the following.

3. Numerical Results

3.1. Surface flow

In this section we describe the pattern of the surface flow of a companion star. The cases of $q = 0.05, 0.33, 0.5, 1, 2,$ and 3 are investigated. The coordinate sizes and number of grid points for each case are listed in Table 1. Note that the case of $q = 1$ was already studied by Oka et al. (2002).

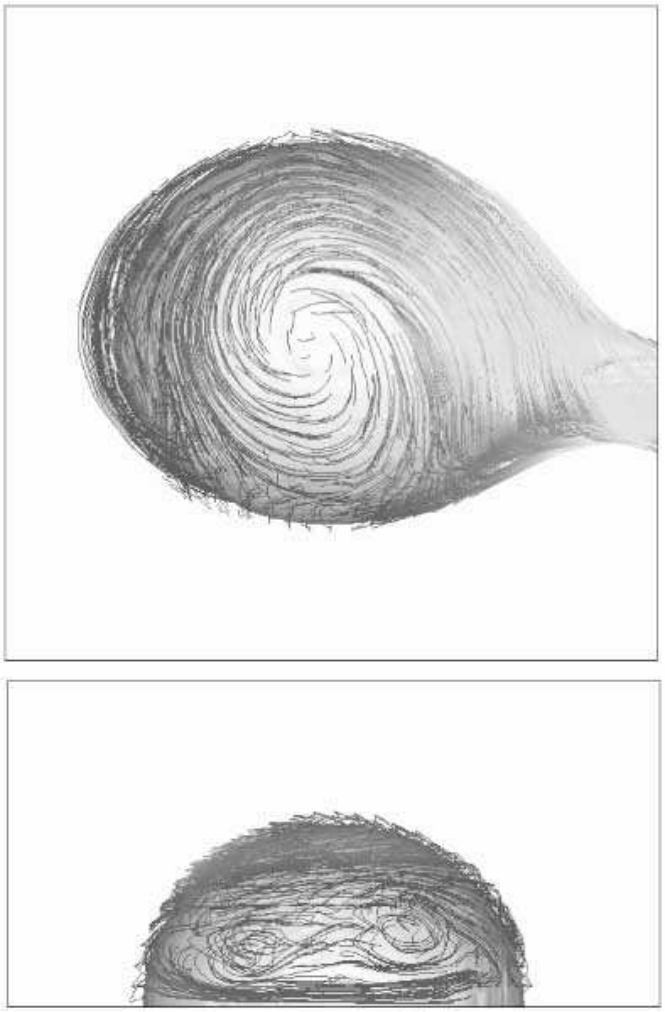

Fig. 2. Equidensity surface ($\log \rho = -2$) of the companion star and the streamlines starting from the equidensity surface of $\log \rho = -2.5$; A mass ratio of $q = 0.33$ and a specific heat ratio of $\gamma = 5/3$, are adopted. The top panel is viewed from the north, while the bottom panel is viewed from the opposite side of the L1-point. H-, L1-, and L2-eddies can be seen.

For the calculation of the surface flow we adopt $\gamma = 5/3$, i.e. we assume adiabatic expansion of the gas in the companion's atmosphere. For the calculation of the accretion discs, on the other hand, we use $\gamma = 1.01$ (almost isothermal) to mimic radiation cooling, necessary to form an accretion disc.

Figure 2 shows an equidensity surface of the companion star and streamlines originating from another equidensity surface, for $q = 0.33$ and $c_0 = 0.05$. We can see the H-, L1-, and L2-eddies as described above; we refer to Oka et al. (2002) for the mechanism of generation of these eddies. It is remarkable that the flow pattern is essentially the same as the case of $q = 1$ in Oka et al. (2002). These eddies are the manifestation of the astrostrophic wind predicted by Lubow & Shu (1975).

Figure 3 depicts the equidensity surface of the accretion disc with $c_0 = 0.05$. We can see a pair of spiral shocks

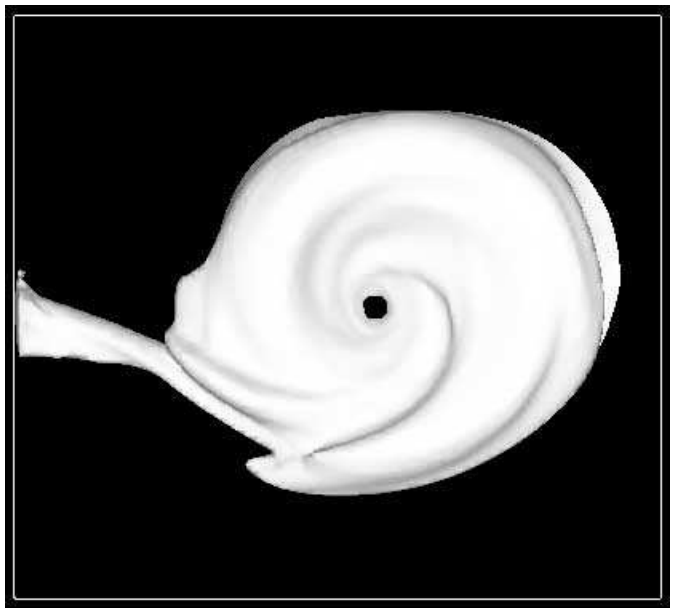

Fig. 3. Equidensity surface ($\log \rho = -3.1$) of the accretion disc is shown; $q = 0.33$ and $\gamma = 1.01$ are adopted in this figure. The size of the whole computed region is $2.0 \times 1.0 \times 0.5$ (including companion star), and the number of grid points is $201 \times 101 \times 51$. Note, however, that the region to the right of the L1 point is shown to exhibit only the accretion disc. We may observe a pair of spiral shocks and a shock associated with the L1 stream.

as well as a shock associated with the L1 stream. Figures 4 and 5 represent the case of $q = 2$ with $c_0 = 0.05$. Compared with Figs. 2 and 3, we observe that the flow pattern is essentially the same as for the lower q case.

Figure 6 shows the result of the extreme mass ratio, $q = 0.05$ with $c_0 = 0.02$. In this case the gravitational potential due to the companion is so shallow that a small fraction of the gas escapes through the L2 point. We do not discuss here this case in detail. We can conclude that the flow pattern does not heavily depend on the mass ratio, q, at least for q greater or of the order of 1.

We note an interesting possibility. As can be seen in Figs. 3 and 5, the equidensity surface rises abruptly behind spiral shocks and is thus making cliffs. These cliffs may be irradiated by the radiation emitted from the central star/the central region of the accretion disc, and thus produce spiral patterns in the Doppler map. We stress here that the spiral shock is a natural consequence of supersonic flow in a non-axisymmetric gravitational potential.

3.2. Construction of Doppler maps

To construct observable Doppler maps, information on the ionisation state of atoms in the photosphere is required, and the ionisation states are mainly determined by the temperature. The temperature in the photosphere of the companion and the accretion disc is affected by the irradiation from the primary and the central part of the

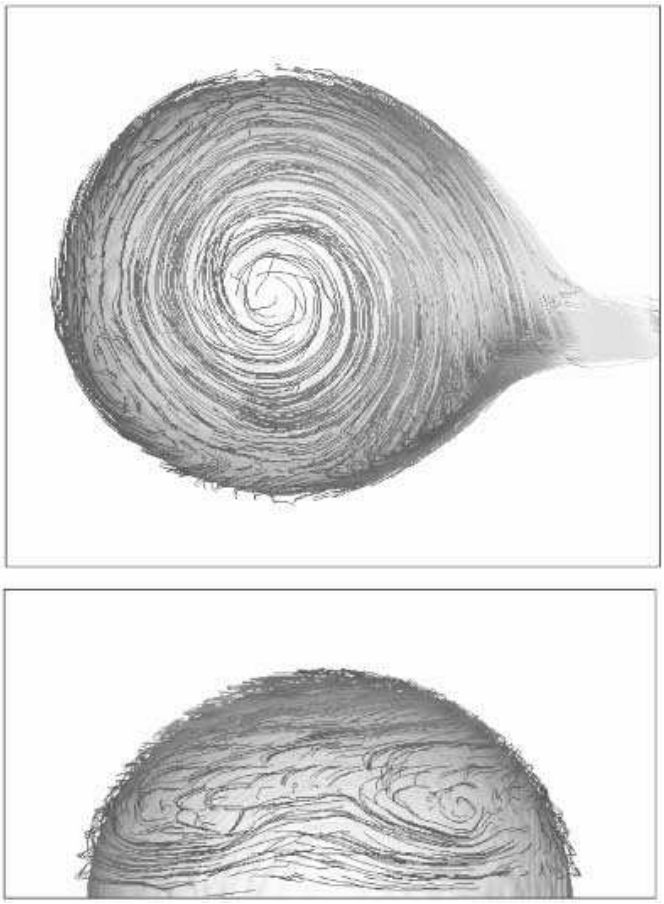

Fig. 4. Same as in Fig. 2 but for a mass ratio of $q = 2$.

Fig. 5. Same as in Fig. 3 but here the equidensity surface of $\log \rho = -4.5$ is shown for a mass ratio of $q = 2$.

Fig. 6. Surface flow on the companion star in a binary with $q = 0.05$; equidensity surface ($\log \rho = -2.5$) of the companion star and the streamlines starting from the equidensity surface of $\log \rho = -3$. Note that a small fraction of the gas flows through the L2 point as well as the L1 point because of the shallow gravitational potential.

accretion disc. Since, in the present study, we do not take the irradiation effect into account, we cannot construct real observable Doppler maps but, instead, we use the following convention.

Instead of identifying a photosphere, we use an equidensity surface as a possible candidate for the photosphere. The horizontal component of gas velocity, $V_{\rm x}$ and $V_{\rm y}$, of each computational cell at that surface is mapped onto a $V_{\rm x} - V_{\rm y}$ plane: the Doppler map. We tested various values of the density and found that the general trend was not affected by a particular choice of the density.

Our construction method of the Doppler map does not reflect the mechanism of line emission, and therefore, only a part of our constructed Doppler map can be observed. For instance the outer (non-irradiated) side of the Roche surface may not be observable, if appropriate lines are not emitted from there.

Another problem in constructing a Doppler map is the choice of γ. We use the case of $\gamma = 5/3$ to calculate the contribution from the companion, while we use the case of $\gamma = 1.01$ for the accretion disc. Thus, we combine two different simulations into one Doppler map. Therefore, we use two different values of density on an equidensity surface: a surface of the companion star and one for the accretion disc. Since our main aim is to investigate Doppler maps caused by the surface flow on the companion, the contribution from the accretion disc should here only be considered as a reference.

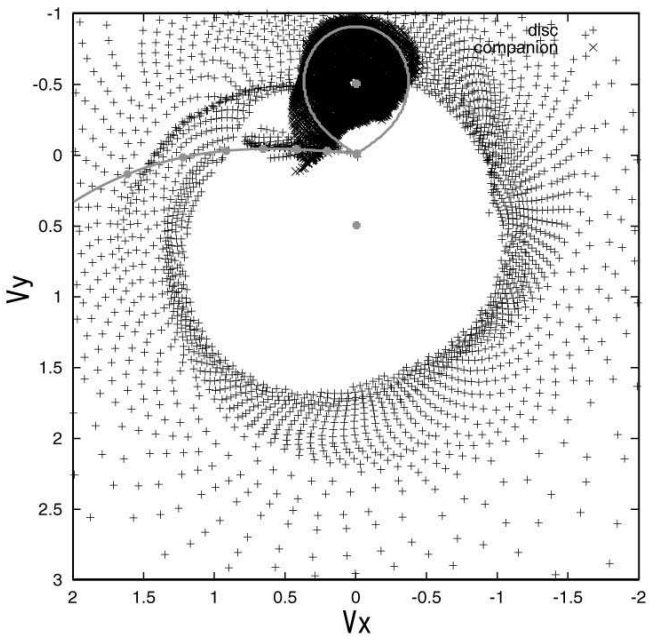

Fig. 7. Doppler map constructed from the horizontal components of velocity, $V_{\rm x}$ and $V_{\rm y}$, at the equidensity surface of $\log\rho = -2.5$ for the companion star (denoted by the cross) and $\log\rho = -3.9$ for the accretion disc (denoted by the plus). In this figure $q = 1$. Note that the following figures are placed upside down in order to compare our results with those of other authors. The critical Roche surface and the ballistic orbit of the L1 stream are also shown for the purpose of reference. The upper and the lower dot show the centre of mass of the companion and that of the primary, while the middle dot (at the L1 point) denotes the common centre of gravity.

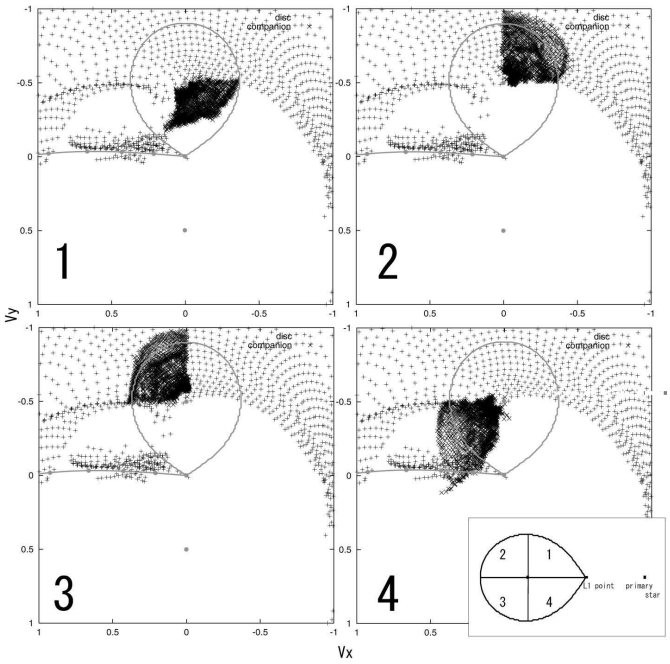

Fig. 8. The surface of the companion is divided into four quadrants as shown in the right bottom sub-panel. We can examine the contribution from each surface region. The number in each Doppler map corresponds to the quadrant in the sub-panel. Note that the same data is used as in Fig. 7.

Figure 7 shows the constructed Doppler map of the equidensity surface of $\log\rho = -2.5$ for the companion star and $\log\rho = -3.9$ for the accretion disc. The mass ratio is $q = 1$ in this case. Note that all the Doppler maps shown in the figures are placed upside-down to accommodate the more common convention used by observers. The critical Roche lobe of the companion star and the ballistic orbit of the L1 stream are also shown for reference purposes. The crosses show the contribution from the companion, while the plus signs show the contribution from the accretion disc, which is just for reference as was described above and we do not give a detailed discussion about this contribution in the present paper. The contribution due to the accretion disc collides with that of the surface flow in the Doppler map. However, this does not necessary mean that the flow in the accretion disc really collides with the companion in the configuration space.

The most important feature in our calculated Doppler maps is the asymmetry about the $V_{\rm y}$-axis. This is due to the surface flow of the companion. If there was no flow on the companion surface, all crosses should reside within the critical Roche surface. However, this is not the case. We can observe that the crosses *deviate* to the upper right and to the lower left.

In order to see this more clearly, Fig. 8 shows the contribution in the Doppler map from each quadrant of the surface region, described by the numbers in Fig. 8. The number in each Doppler map corresponds to the quadrant labeled by the same number in the right bottom sub-panel. One may safely speculate that the asymmetries seen in quadrant 1 and in quadrant 4 are due to the flow in the L1-eddy. The deviations seen in quadrants 2 and 3 are due to the L2-eddy, although this portion of the Doppler map is unobservable because of lack of irradiation.

We may summarize the characteristics of the Doppler map due to the companion as follows:

1. The velocity vector denoted by 1 in Fig. 1 has a contribution of positive $V_{\rm x}$, $V_{\rm y}$. This produces the asymmetries.
2. The velocity vector denoted by 2 has a contribution of positive $V_{\rm x}$ and negative $V_{\rm y}$.
3. The velocity vector denoted by 6 has a contribution of negative $V_{\rm x}$ and $V_{\rm y}$.
4. The velocity vector denoted by 7 has a contribution of positive $V_{\rm x}$ and negative $V_{\rm y}$.
5. Velocity vectors associated with the H-eddy, i.e. 3, 4 and 5, have a tendency to shrink the cross dots in the companion towards the centre of the companion.

4. Supersoft X-ray sources

We apply our results to the Galactic supersoft X-ray source: RX J0019.8+2156 and try to attribute the low radial velocity component of the emission lines of He II λ4686 in the Doppler map observed by Deufel et al. (1999) to the irradiated spot on the surface of the companion.

Figure 9 shows our constructed Doppler map with $q = 3$, as a model for the RX J0019.8+2156. We assume the system velocity to be $A\Omega_{\rm orb} = 330$km/s. The equidensity surface is chosen with $\log\rho = -2.5$ for the companion and $\log\rho = -4.4$ for the accretion disc. The region where a strong He II λ4686 emission line peak around $V_{\rm x}\sim$ 100 km/s and $V_{\rm y}\sim$ 100 km/s (with our velocity convention) is observed by Deufel et al. (1999), is denoted by a dotted circle.

From Fig. 9, we may conclude that the case of $q \sim 3$ can naturally explain the low radial velocity component of the emission lines of He II λ4686. This is the same result as obtained by Hachisu & Kato (2003). The mass ratio, $q \sim 3$, means that the mass of the companion star is larger than that of the white dwarf. Considering that a mass above $\sim 0.8M_\odot$ for the WD is ruled out by its relatively low X-ray flux of $\sim 0.4\times10^{37}$ergs/s (Beuermann et al. 1995; Meyer-Hofmeister et al. 1998), we may assume the mass of the white dwarf to be $\sim 0.6M_\odot$. Therefore, the mass of the companion star can be estimated to be $\sim 2M_\odot$.

Finally, as was discussed earlier, the emission peak as denoted by the dotted circle is due to the L1-eddy, and if so, we may say that the Doppler map obtained by Deufel et al. (1999) exhibits the trace of the surface flow on the companion star.

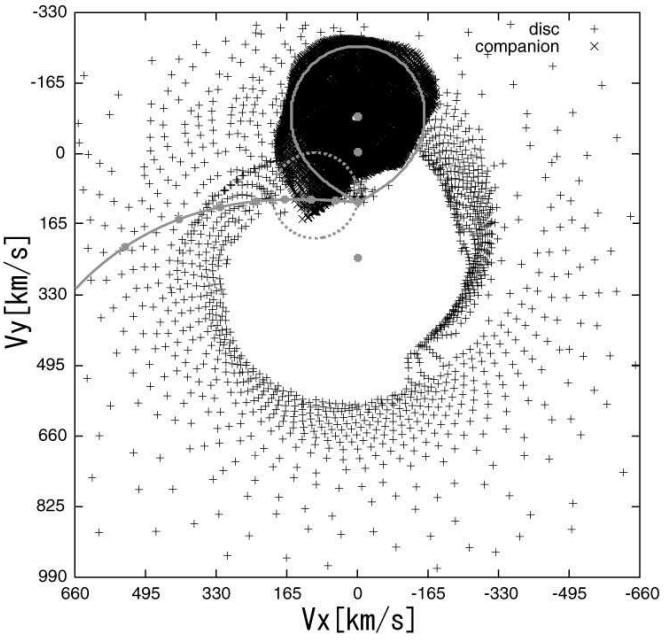

Fig. 9. Constructed Doppler map as a model of the RX J0019.8+2156 with $q = 3$: in order to have a velocity scale, we assume $A\Omega_{\rm orb} = 330$ km/s. The observed intensity of the He II λ4686 emission by Deufel et al. (1999) has a peak around $V_{\rm x} \sim 100$ km/s and $V_{\rm y} \sim 100$ km/s (in our velocity sign), denoted here by a dotted circle.

5. Summary

We investigate the surface flow of the companion star in a semi-detached binary system and construct model Doppler maps. Six cases with mass ratios of $q = 0.05, 0.33$, 0.5, 1, 2, and 3 are considered. We apply our results to the Galactic supersoft X-ray source RX J0019.8+2156. The results are summarized as follows:

1. We obtain the H-, L1-, and L2-eddies, which were found by Oka et al. (2002), for all mass ratios. We confirm that the flow pattern does not heavily depend on the mass ratio.
2. We construct model Doppler maps, and we find an asymmetric velocity distribution, due to the surface flow.
3. The companion mass of RX J0019.8+2156 is estimated to be around $2M_\odot$. This massive companion is consistent with the theoretical model proposed by van den Heuvel et al. (1992).
4. We argue that the Doppler map of supersoft X-ray sources shows indications of the surface flow on the companion star.

Acknowledgements. The authors would like to thank an anonymous referee for useful suggestions and comments. K.O. was supported by the Research Fellowships of the Japan Society for Promotion of Science for Young Scientists. T.M. was supported by the grant in aid for scientific research of Japan Society of Promotion of Science (13640241). This work was supported by "The 21st Century COE Program of Origin and Evolution of Planetary Systems" in Ministry of Education, Culture, Sports, Science and Technology (MEXT). Calculations were carried out on the SGI Origin 3800 at the Information Science and Technology Center of Kobe University.

References

Becker, C. M., Remillard, R. A., Rappaport, S. A., & McClintock, J. E. 1998, ApJ, 506, 880

Beuermann, K., Reinsch, K., Barwig, H., Burwitz, V., de Martino, D., Mantel, K.-H., Pakull, M. W., Robinson, E. L., Schwope, A. D., Thomas, H.-C., Truemper, J., van Teeseling, A., Zhang, E. 1995, A&A, 294, L1

Cowley, A. P., Schmidtke, P. C., Crampton, D., & Hutchings, J. B. 1998, ApJ, 504, 854

Davey, S. C., & Smith, R. C. 1992, MNRAS, 257, 476

Davey, S. C., & Smith, R. C. 1996, MNRAS, 280,481

Deufel, B., Barwig, H., Šimić, D., Wolf, S., & Drory, N. 1999, A&A, 343, 455

Dhillon, V. S., & Watson, C. S. 2000, Proc. of the Astrotomography Workshop, Brussels, July 2000, ed. H. Boffin, & D. Steeghs (Springer-Verlag Lecture Notes in Physics), 94

Fujiwara, H., Makita, M., Nagae, T., & Matsuda, T. 2001, Progr. of Theor. Phys., 106, 729

Gänsicke , B. T., van Teeseling, A., Beuermann, K., & Reinsch, K. 2000, New Astr. Rev., 44, 143

Hachisu, I., & Kato, M. 2003, ApJL, submitted
Jyounouchi, T., Kitagawa, S., Sakashita, S., & Yasuhara, M. 1993, Proc. 7th CFD Symp.
Lubow, S. H., & Shu, F. H. 1975, ApJ, 198, 383
Makita, M., Miyawaki, K., & Matsuda, T. 2000, MNRAS, 319, 906
Matsuda, T., Makita, M., Fujiwara, H., Nagae, T., Haraguchi, K., Hayashi, E., & Boffin, H. M. J. 2000, Ap&SS, 274, 259
Matsumoto, K., & Mennickent, R. E. 2000, A&A, 356, 579
McGrath, T. K., Schmidtke, P. C., Cowley, A. P., Ponder, A. L., & Wagner, R. M. 2001, AJ, 122, 1578
Meyer-Hofmeister, E., Schandl, S., Deufel, B., Barwig, H., & Meyer, F. 1998, A&A, 331, 612
Oka, K., Nagae, T., Matsuda, T., Fujiwara, H., & Boffin, H. M. J. 2002, A&A, 394, 115
Shima, E., & Jyounouchi, T. 1994, NAL-SP27, Proc. of 12th NAL Symp. on Aircraft Computational Aerodynamics, 255
van den Heuvel, E. P. J., Bhattacharya, D., Nomoto, K., & Rappaport, S. 1992, A&A, 262, 97
Watson, C. A., Dhillon, V. S., Rutten, R. G. M., & Schwope, A. D. 2003, MNRAS, 341, 129